



Effect of Microstructure Refining on the Thermal Stability and Wear Resistance of Abradable AlSi-Polyester Coating

Jian-jiang Tang¹ · Fang-li Yu¹ · Hai-hong Zhang¹ · Dan Chen¹

Submitted: 12 July 2020 / in revised form: 21 April 2021 / Accepted: 10 May 2021 / Published online: 8 June 2021
© ASM International 2021

Abstract Abradable coatings are used in gas turbines to minimize the clearance distance between the stationary components and rotating blade tips. In this study, the effect of microstructure refining on the properties of abradable AlSi-polyester coatings was investigated. The coatings were deposited by conventional atmospheric plasma spraying system (APS) and high efficiency supersonic atmospheric plasma spraying system (SAPS). The results showed that the average area of single polyester phase was $351 \pm 27 \mu\text{m}^2$ in SAPS coating, about 25.2% lower than that of APS coating ($469 \pm 22 \mu\text{m}^2$). The hardness and bonding strength of as-sprayed SAPS coating were 79 HR15Y and 15.2 MPa, respectively, about 16.2 and 28.8% higher than the hardness and bonding strength of as-sprayed APS coating (68 HR15Y and 11.8 MPa). The track depth and friction coefficient of SAPS coating were about 51.1 and 16.9% lower than those of APS coating. When the coatings were subjected to hot-corrosion and thermal shock tests, the hardness and bonding strength of SAPS coating (47 HR15Y and 6.3 MPa) were about 67.9 and 200% higher than those of APS coating (28 HR15Y and 2.1 MPa). Additionally, the track depth and friction coefficient of SAPS coating were about 61.3 and 12.1% lower than those of APS coating. This work shows that the refinement of polyester phase, low porosity and less amount of Si phase precipitation were beneficial to improve the thermal stability and in-service performance of the abradable AlSi-polyester coatings.

Keywords abradable coatings · AlSi-polyester · plasma spraying · microstructure refining · thermal stability · wear resistance

Introduction

Abradable coatings are utilized as sacrificial materials in low pressure compressor casings, and in intermediate and high pressure compressors and seals (Ref 1). The main purpose of this contribution is to minimize the clearance distance between the stationary components and rotating blade tips, resulting in higher performance and lower fuel consumption (Ref 2-4). Considering the harsh working conditions of the abradable coatings, many excellent properties should be provided for the substrate, including bonding strength, thermal stability, corrosion resistance, and tribologic properties, et al (Ref 3, 5, 6).

AlSi-polyester abrasives are used for titanium compressor casings of the engine for temperatures up to 325 °C, due to the high temperature limit posed by the melting temperature of the polymer (Ref 1, 7). The present researchers have mainly paid attention to the effect of spray processes, porosity, temperature, and thermal aging-erosion on the properties of AlSi-polyester abradable coatings (Ref 1, 2, 8-10). However, the effect of lubricating phase refinement on performance has not attracted much attention. Previous results have shown that the fine distribution of the lubricating phase can effectively improve the friction properties of the coating (Ref 11, 12).

The air plasma spraying (APS) system is commonly used to deposit the AlSi-polyester coating, due to its simple operation and high efficiency. The hardness and porosity of the coatings can be controlled by changing the spray parameters (Ref 2, 13). As compared to APS, the high

✉ Jian-jiang Tang
tangjianjiang@xau.edu.cn

¹ School of Materials Engineering, Xi'an Aeronautical University, Xi'an 710077, People's Republic of China

efficiency supersonic atmospheric plasma spraying (SAPS) system can get a denser coating and also refine the coating structure (Ref 11, 12, 14, 15).

This work was carried out aimed to further understand the effect of microstructure refining of the lubricating phase on the thermal stability of AlSi-polyester coating, and ultimately to improve their in-service performance.

Experimental

Materials

The substrate, IN718 with the dimension of $40 \times 30 \times 5 \text{ mm}^3$, was ultrasonically cleaned with acetone and then grit-blasted with alumina powder to enhance the adherence capability between bond coat and substrate. The abrasible coating system consisted of a bond coat (transition layer) and a top coat (abrasible layer). A commercially available Ni_{35}Cr powder (Beijing Yi Xin An Technology Development Co., Ltd, China) was used as the bond coat material. METCO 601NS AlSi-polyester powders (40 wt.% polyester + 60 wt.% Al12Si alloy, M601) was used as the top coat material. The morphology of Ni_{35}Cr and M601 powders is shown in Fig. 1. As depicted, the feedstock powders exhibited an irregular shape and a non-uniform particle size distribution. The M601 powders were fabricated by blending Al-Si alloy powders and polyester powders.

Plasma Spraying

The AlSi-polyester coatings were deposited by the Metco 9MB air plasma spraying (APS) system and the high efficiency supersonic atmospheric plasma spraying (SAPS) system, respectively. The plasma spraying parameters are presented in Table 1. During spraying, a commercially available Spray Watch 2i system (made by Osier, Finland) was used to monitor the velocity and surface temperature of in-flight particles for each operating condition.

Specimen Characterization

The microstructure of AlSi-polyester coatings was examined by scanning electron microscopy (SEM, VEGAII XMU, Tescan, Czech Republic). The content and size of polyester phase in coatings were calculated by quantitative image analysis, using an Image-Pro Plus software (Media Cybernetics, Silver Springs, MD). The final statistical result was the average value from ten micrographs of the coatings. The phase composition of coatings was characterized by x-ray diffraction (XRD, D/MAX-2400X, Rigaku, Japan) using $\text{Cu K}\alpha$ radiation ($\lambda = 0.15406 \text{ nm}$), the angle in the range of $15\text{--}80^\circ$, the step size at 0.008° .

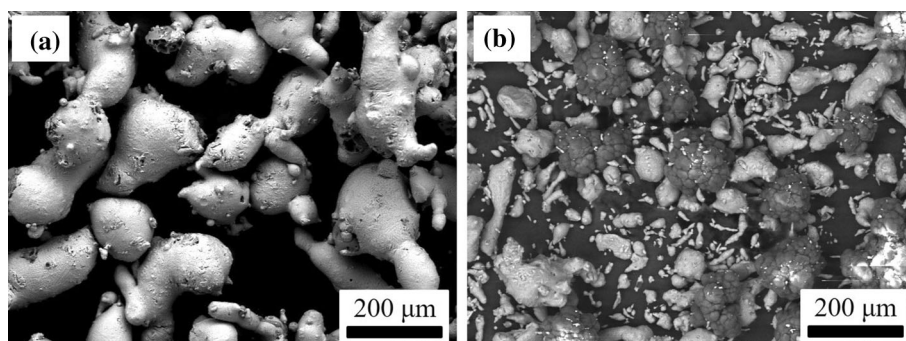
Performance Tests

The bonding strength of AlSi-polyester coatings was measured by using a materials tester (Instron1196, USA) in accordance with ASTM C633-79 standard. The film epoxy adhesive (FM1000, USA) was used to bond the samples. The final result represented the average value of five coatings deposited at the same parameters. The hardness was tested by the commonly used HR15Y tester (HSRN-45, Wuzhong City Material Testing Machine Co., Ltd., China). The polished surface of the coating was measured

Table 1 Plasma spraying parameters

Spraying parameters	APS (9M)		SAPS	
	Ni_{35}Cr	M601	Ni_{35}Cr	M601
Primary gas Ar, slpm	48	90	71	70
Second gas H_2 , slpm	4.6	4.2	9	10.2
Powder feed rate, g/min	40	40	40	40
Voltage, V	70	67	120	130
Current, A	500	400	380	380
Spray distance, mm	100	100	100	100

Fig. 1 Appearance of raw material powders: (a) Ni_{35}Cr , (b) M601



10 times in different areas with a load of 150 N and a holding time of 3 seconds.

The hot-corrosion resistance of AlSi-polyester coatings was measured by acid vapor for a simulated environment. The corrosive liquid was prepared by 50% acetic acid (concentration 36%) + 50% distilled water, which was heated to above 100 °C to produce acid vapor. The acid vapor passed into an alumina tube at a temperature of 250 °C, while the samples were subjected to an acid corrosion test. The thermal shock test was carried out based on the hot-corrosion test. The thermal shock test specimens were kept for 10 min at 300 °C, and then the coatings were quickly cooled to 20–30 °C by compressed air. The thermal shock test was stopped when the number of cycles has reached 300.

The friction coefficients of AlSi-polyester coatings were evaluated by the ball-on-flat mode on the UMT-3 friction and wear tester (CETR Corporation Ltd, USA) with the reciprocating and sliding wear method. The counter-wear was a 440-C stainless steel ball with the diameter of Φ 12.7 mm and the hardness of HRC 62. The tests were carried out for 60 N with the reciprocating and sliding wear method and without lubricant at room temperature (about 25 °C), sliding a distance of 10 mm per pass with the frequency of 10 Hz, and sliding time of 30 min. The friction coefficient and the track depth of the test were recorded automatically by a computer in the test process. After the test, the worn surface morphologies of coatings were observed by SEM.

Results and Discussion

Microstructural Characterization

Figure 2 shows the XRD patterns of the feedstock powder and as-sprayed coatings. As seen from Fig. 2, the diffraction peaks consisted of polyester, SiO₂, Al, and Si phases. The APS coating showed obvious diffraction peaks of Si phase compared to feedstock powder and SAPS coating.

Figure 3 depicts the typical morphologies of flattened APS-/SAPS-particles. As shown in Fig. 3, compared with the central distribution of APS-particles, the SAPS-particles were dispersively distributed. It was found that the size of single phase was significantly decreased compared with APS-particles. Figure 4 depicts the polished cross-sectional morphology of as-sprayed coatings. As seen from Fig. 4, the black area was polyester phase and the bright area was Al-Si matrix. In the APS coating, some pores (see yellow arrow) were found in the microstructure. In comparison, the size of polyester phase was smaller and less pores exist in the structure of SAPS coating. The size of polyester phase and porosity in the coatings were calculated by quantitative image analysis. The statistical results showed that the porosities were $0.25 \pm 0.08\%$ in SAPS coating and $0.90 \pm 0.08\%$ in APS coating, respectively. Meanwhile, the average area of single polyester phase was $351 \pm 37 \mu\text{m}^2$ in SAPS coating, which was about 25.2% lower than that of APS coating ($469 \pm 42 \mu\text{m}^2$). Furthermore, the area ratios of the polyester phase were $53.9 \pm 0.2\%$ in SAPS coating and $54.1 \pm 0.3\%$ in APS coating.

As seen from the partial enlarged detail (Fig. 4c, d), for APS coating, more small bright white dots were found in the Al-Si matrix compared to SAPS coating. The EDS results (see Fig. 5) showed that the small bright white dots were Si phase. According to the binary phase diagram of Al-Si alloy (Ref 16), Al phase and Si phase do not react to form a compound, but only a solid solution. Al phase is almost insoluble in Si phase, while the solid solubility of Si phase in α -Al matrix under equilibrium solidification condition is about 1.59%. When Al-Si alloy powders were deposited by plasma arc to form coating, the solid solubility of Si phase was greatly improved with the non-equilibrium condensation conditions (Ref 17). A plasma-sprayed coating was formed through successive impact, flattening, rapid cooling and solidification processes of a stream of in-flight particles. The microstructure of as-sprayed coating was closely linked with the morphology of single flattened particle, which was mainly determined by the in-flight speed of the particles.

The average velocity and surface temperature of in-flight M601 particles were measured by Spray watch 2i

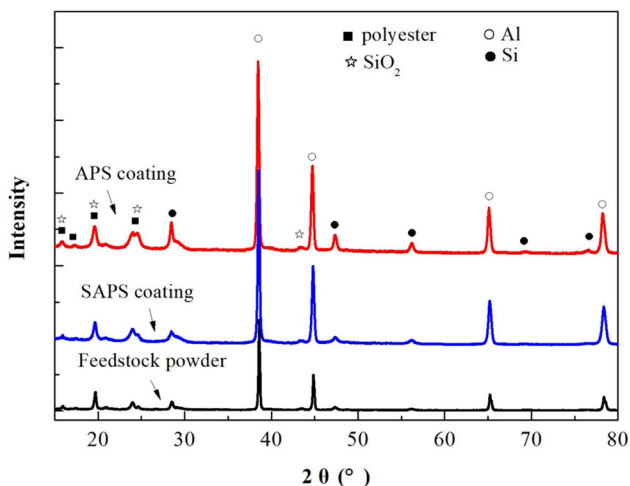


Fig. 2 The XRD patterns of the feedstock powder and as-sprayed coatings

Fig. 3 The typical morphologies of flattened APS-/SAPS-particles: (a) flattened SAPS-particles, (b) flattened APS-particles

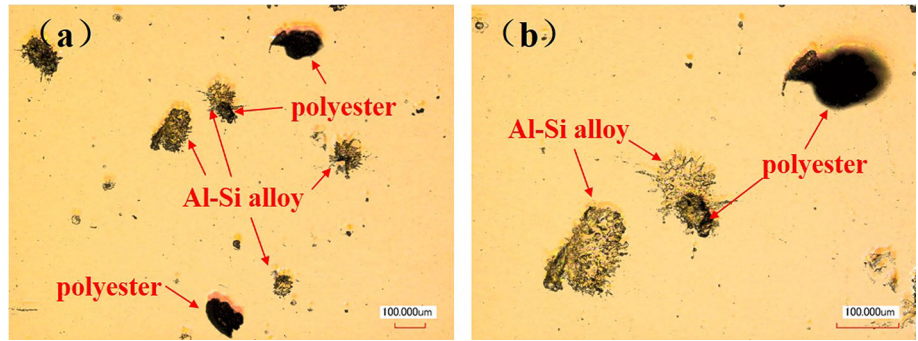


Fig. 4 Cross-sectional SEM images of as-sprayed coatings: (a) (c) SAPS coating, (b) (d) APS coating

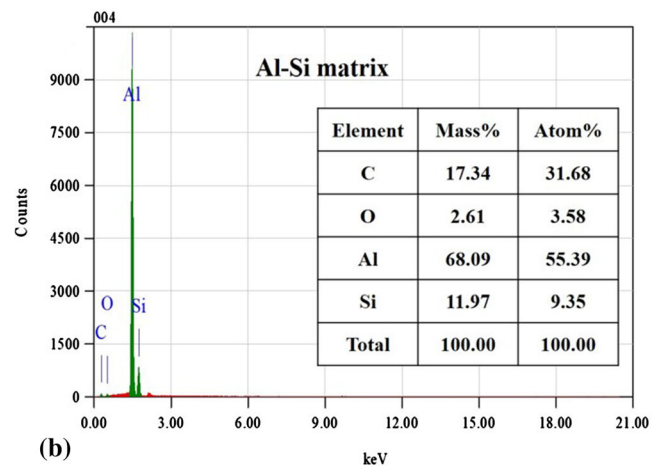
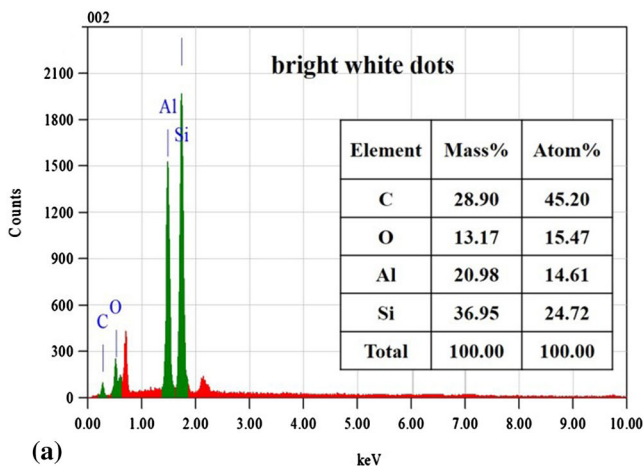
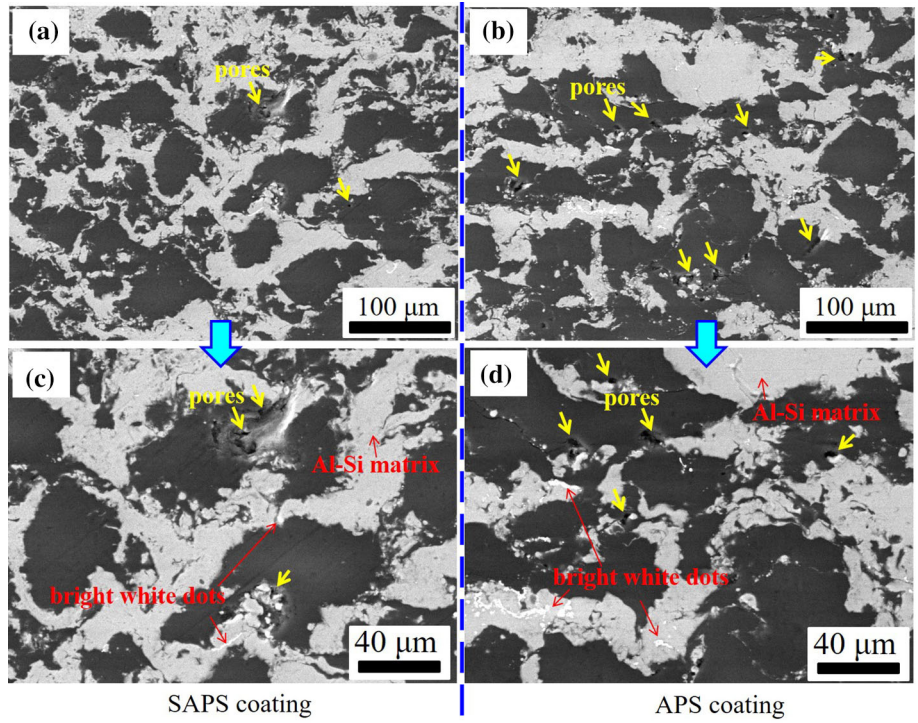
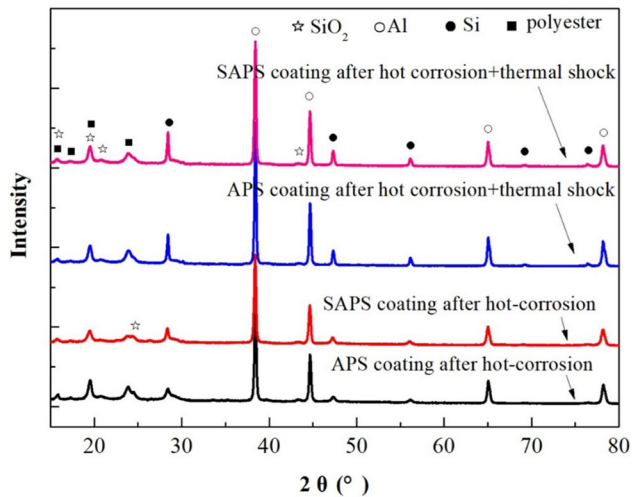


Fig. 5 Energy spectrum results of bright white dots and Al-Si matrix.

Table 2 Average velocity and surface temperature of in-flight M601 particles measured by spray watch 2i system.

In-flight properties	APS	SAPS
Average velocity, m/s	179	472
Average surface temperature, °C	2060	2134

**Fig. 6** The XRD patterns of coatings after hot-corrosion/thermal shock tests

system (see Table 2). The results showed that the velocity of particles in SAPS plasma jet was 472 m/s, about 2.6 times higher than that of APS (179 m/s). The higher speed resulted in increased flatness of in-flight particles and the dispersion of polyester phase, leading to the faster cooling rate of flattened particle, denser structure and smaller size of polyester phase of coating. Additionally, for SAPS coating, the faster cooling rate of flattened particle kept a higher solid solubility of Si phase in α -Al matrix.

Figure 6 shows the XRD patterns of coatings after tests. As seen from Fig. 6, the diffraction peaks of coatings after tests consisted of polyester, SiO₂, Al, and Si phases. For the coatings after hot-corrosion and thermal shock, the diffraction peaks of Si phase were higher than that of the coatings after hot-corrosion. The Al-Si alloy structure of as-sprayed coatings is in a metastable state attributed to the rapid cooling rate of flattened particle. When subjected to heat treatment, the Al-Si alloy structure changed to a stable state. At the same time, the Si phase in the supersaturated solid solution precipitated from the α -Al matrix, resulting in the Si particles content increased with the heating time increasing at high temperature.

Figure 7 shows the polished cross-sectional morphology of coatings after tests. As seen from Fig. 7, according to the polished cross-sectional morphology, the polyester

appeared to be missing in the coatings after thermal treatments, especially after the thermal shock test at 300 °C. After subjected to hot-corrosion test, some pores (yellow arrow) were generated between the metal matrix phase and the polyester phase (see Fig. 7a and b). For the APS coating, more pores appeared and the size of pores was larger than that of SAPS coating. A small volume shrinkage of polyester was caused by the thermal flow at 250 °C, resulting in the pores formation. Additionally, the thermal flow and corrosive media could extend into the coatings along the pores created by the shrinkage of polyester. The interface between the matrix phase and polyester phase was corroded, and then more volume shrinkage of polyester appeared. After the thermal shock test, the structure of coatings suffered severe damage, manifested by the increase in the number and size of pores in the coatings. The pores were produced not only between the metal matrix phase and the polyester phase, but also found within the polyester phase (see Fig. 7c and d).

Compared to SAPS coating, the size of pores was larger and the damage of coating structure became more serious in APS coating after hot-corrosion test. At first, the coatings were subjected to a combined action of high temperature and alternating stress during thermal shock test. The ablation and volume shrinkage of polyester phase was exacerbated at 300 °C, resulting in more and larger pores formation. Meanwhile, the air in the pores and the gas generated by the ablation of polyester phase escaped outward when heated, resulting in a destructive effect on the structure of the coating. Secondly, the alloy matrix phase and polyester phase were combined by mechanical occlusion in the coatings. The thermal expansion coefficient and thermal conductivity were quite different between the different phases. For the thermal expansion coefficient, the Al-Si alloy was about $1.88 \times 10^{-5} \text{ K}^{-1}$ and polyester phase was about $3.1 \times 10^{-5} \text{ K}^{-1}$. Therefore, it was easy to cause the crack initiation and expansion at the two-phase interface by the function of alternating stress in the thermal shock process. Finally, the thermal flow quickly diffused into the interior of the coating along the cracks and pores. As a result, more polyester was ablated and severe two-phase separation happened.

Hardness and Bonding Strength

Figure 8 shows the hardness and bonding strength of coatings before and after tests. As seen from Fig. 8, the results showed that the values of hardness and bonding strength decreased as the tests were carried out. During the bonding strength test, samples fractured inside the coatings. For the as-sprayed coating, the hardness and bonding strength of SAPS coating were 79 HR15Y and 15.2 MPa, about 16.2 and 28.8% higher than those of APS coating,

Fig. 7 The polished cross-sectional morphology of (a) SAPS coating after hot-corrosion test, (b) APS coating after hot-corrosion test, and (c) SAPS coating after hot-corrosion + thermal shock tests, (d) APS coating after hot-corrosion + thermal shock tests

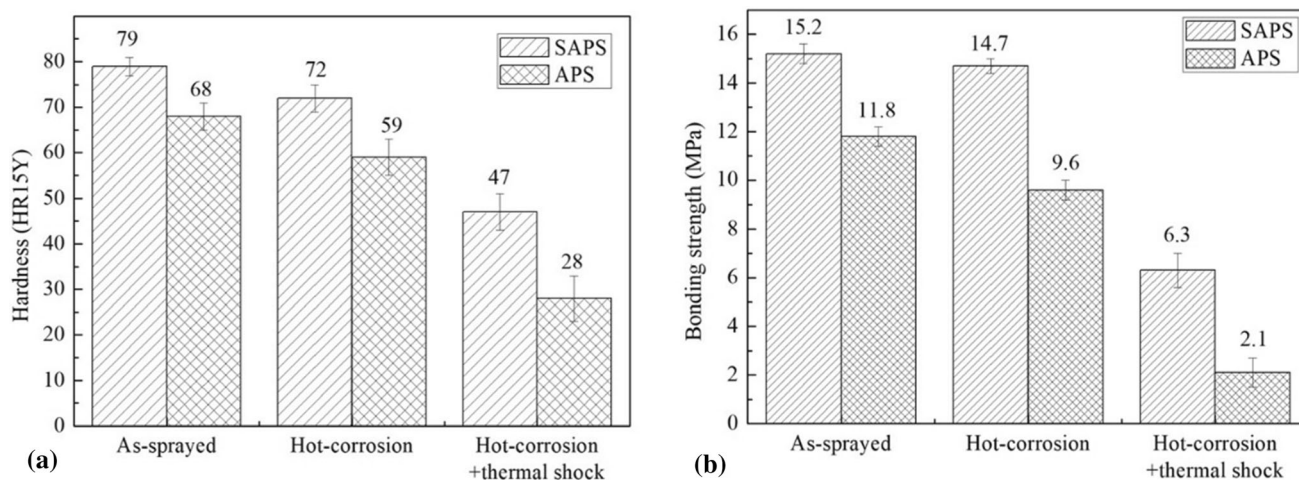
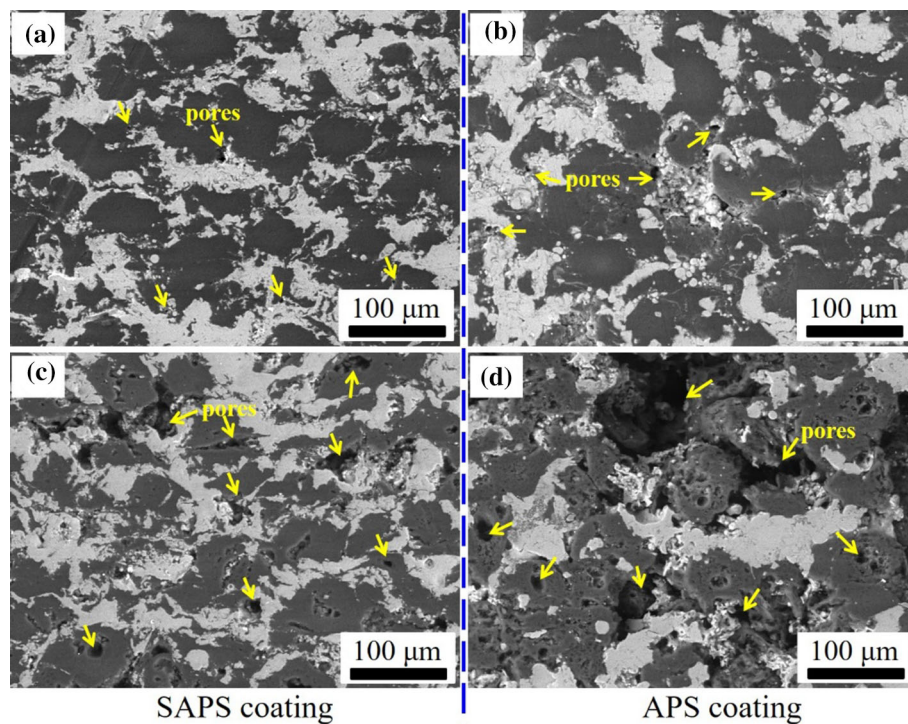


Fig. 8 The statistical results of (a) hardness, (b) bonding strength before and after tests.

respectively. The results were attributed to the higher in-flight velocity of particles, which increased the interlamellar bonding area and the density of coating. After the hot-corrosion test, compared to as-sprayed coatings, the hardness (72 HR15Y) and bonding strength (14.7 MPa) of SAPS coating were reduced about 8.9 and 3.3%, respectively, while the reduction of those in APS coating was up to 13.2% (59 HR15Y) and 18.6% (9.6 MPa). When the thermal shock test was further carried out based on the hot-corrosion test, the values of hardness and bonding strength were sharply reduced. For the SAPS coating, the hardness and bonding strength were 47 HR15Y and 6.3 MPa,

respectively, about 40.5 and 58.6% lower than that of as-sprayed SAPS coating. For the APS coating, the hardness and bonding strength were 28 HR15Y and 2.1 MPa, and the reduction was about 58.8 and 82.2% compared with as-sprayed APS coating. Furthermore, the values of hardness and bonding strength of APS coating after tests were only 59.6 and 33.3% of that in SAPS coating, respectively. The results showed that the thermal stability of SAPS coating was better than that of APS coating.

During thermal shock, the polyester phase was continuously ablated and decomposed, resulting in the destruction of the honeycomb structure of polyester phase, which

was uniformly embedded in the Al-Si alloy skeleton. Meanwhile, the Si phase precipitated from the α -Al matrix and caused the structure of Al-Si matrix to become loose. Therefore, a large number of microscopic defects were generated in the coating, which created the conditions for crack initiation and expansion. The hardness and bonding strength of coatings decreased significantly with the increase in defects.

Friction Performance

Figure 9 depicts the friction curves of the coatings before and after tests. As seen from Fig. 9, the friction curve of as-sprayed SAPS coating was smoother and lower than that of as-sprayed APS coating. After the hot-corrosion and thermal shock tests, the coefficient values and volatility of the friction curves increased. At this point, the friction curve of the SAPS coating was still lower than that of APS coating.

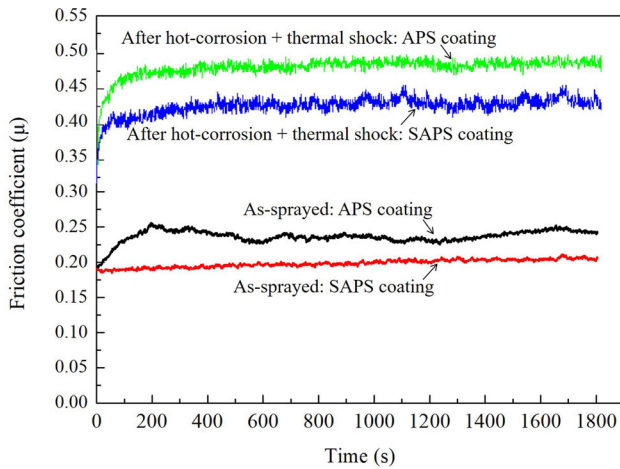


Fig. 9 The friction curves of coatings before and after tests.

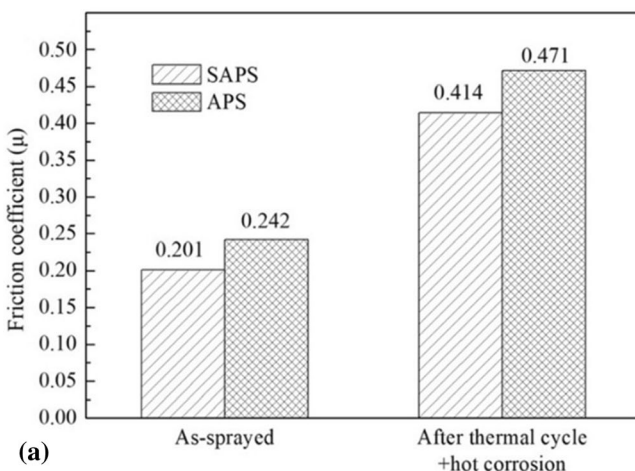


Figure 10 shows the statistical results of friction coefficients and the track depths of coatings before and after shock test. As seen from Fig. 10a, the statistical results showed that the value of friction coefficient of as-sprayed SAPS coating were 0.201, about 16.9% lower than that of APS coating (0.242). The values of friction coefficient of coatings after tests were twice higher than that of as-sprayed coatings. After tests, the value of friction coefficient of SAPS coating was still 12.1% lower than that of APS coating. As seen from Fig. 10b, the track depths of coatings increased after hot-corrosion and thermal shock tests. For the as-sprayed coatings, the track depth of as-sprayed APS coating (0.352 mm) was about double as deep as that of SAPS coating (0.172 mm). Subsequently, the track depth of APS coating increased sharply after tests (1.283 mm) compared with the as-sprayed APS coating, about 158.7% higher than that of SAPS coating (0.496 mm). The above results showed that the SAPS coating exhibited a better lubricity and higher wear resistance compared to the APS coating.

Figure 11 depicts the worn surface morphologies of coatings before and after tests. As depicted in Fig. 11, the worn surface of as-sprayed coatings was smooth, and some fine wear debris was found on the worn surface of the coatings after tests. As compared to SAPS coating, the plastic flow layer was found on the worn surface of as-sprayed APS coating, and more wear debris was produced on the worn surface of APS coating after tests.

For the APS coating, the structure was more porous and weak, resulting in lower bonding strength compared with the SAPS coating. In the reciprocating and sliding wear process, the structure of APS coating was more easily broken and dragged, resulting in more mixture of Al-Si matrix and polyester phase produced. The viscosity of the mixture was higher than that of the pure polyester phase, leading to an increase in friction coefficient. Meanwhile,

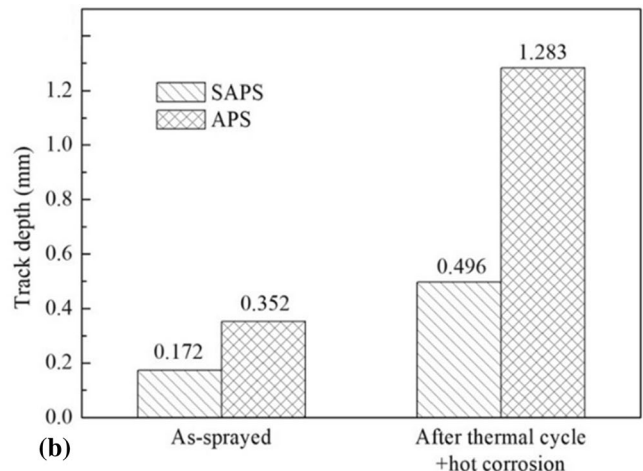
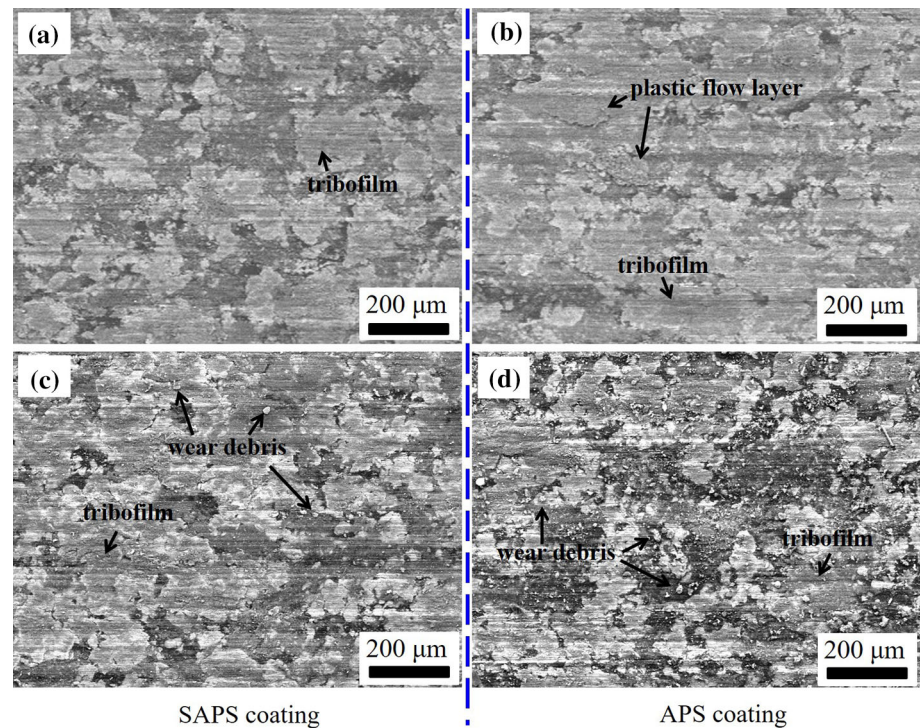


Fig. 10 The statistical results of friction coefficients and the track depths of coatings before and after tests.

Fig. 11 Worn surface morphologies of (a) as-sprayed SAPS coating, (b) as-sprayed APS coating, and after hot-corrosion and thermal shock tests (c) SAPS coating, (d) APS coating.



the plastic spreading of the mixture was reduced, which caused the formation of wear debris. On the other hand, the honeycomb structure in the coatings had been severely damaged after hot-corrosion and thermal shock tests, and the bonding strength and hardness both reduced. Therefore, in the friction process, the more severe damage of the coating structure appeared would cause greater scratch depth.

Conclusions

In this study, the effect of microstructure refining on the properties of hardness, bonding strength, hot-corrosion resistance, thermal shock resistance and wear resistance of AlSi-polyester coatings was investigated. The results indicated that the SAPS coating had better comprehensive properties than that of APS coating. The details are as following:

- (1) Compared to the as-sprayed SAPS coating, more Si phase precipitated from the metal matrix, some pores were found in the as-sprayed APS coating. Meanwhile, the average area of single polyester phase was $469 \pm 22 \mu\text{m}^2$ in the APS coating, about 33.6% higher than that of SAPS coating ($351 \pm 27 \mu\text{m}^2$). The area ratios of the polyester phase were $53.9 \pm 0.2\%$ in SAPS coating and $54.1 \pm 0.3\%$ in APS coating.
- (2) When the coatings were subjected to hot-corrosion and thermal shock tests, the ablation and volume shrinkage of polyester phase became more obviously in APS coating compared with SAPS coating.
- (3) For the as-sprayed coating, the hardness and bonding strength of SAPS coating were 79 HR15Y and 15.2 MPa, about 16.2 and 28.8% higher than those of APS coating (68 HR15Y and 11.8 MPa), respectively. After hot-corrosion and thermal shock tests, the hardness and bonding strength in SAPS coating were about 40.5 and 58.6% lower than those of the as-sprayed SAPS coating. Meanwhile, the hardness and bonding strength of APS coating were about 58.8 and 82.2% lower than those of as-sprayed APS coating. What's more, the hardness and bonding strength of APS coating after tests were only 59.6 and 33.3% of those in the SAPS coating, respectively.
- (4) For the as-sprayed SAPS coatings, the track depth and friction coefficient were 0.172 mm and 0.201, about 51.1 and 16.9% lower than those of as-sprayed APS coating. When the coatings were subjected to hot-corrosion and thermal shock tests, the track depth and friction coefficient of SAPS coating were 0.496 mm and 0.414, respectively, about 61.3 and 12.1% lower than those of APS coating.
- (5) The above results indicated that the refinement of polyester phase, low porosity and less amount of Si phase precipitation was beneficial to improve the

thermal stability and wear resistance of AlSi-polyester coating.

Acknowledgments This work was supported by the Natural Science Basic Research Plan in Shaanxi Province of China (Grant No. 2020JQ-911, 2020JM-631, 2019JQ-910), and Natural Science Foundation of China (Grant No.51902241).

References

1. A. Pellegrino, P.M. Maria Jesus, K. Dragnevski, G. Zumpano and N. Petrinic, Temperature and Strain Rate Dependent Mechanical Response of METCO 601 Aluminium-Polyester Abradable Seal Coating, *EPJ Web Conf.*, 2018, **183**(04012), p 1–6.
2. D. Jech, L. Čelko, P. Komarov, J. Ziegelheim, Z. Česánek and J. Schubert, The Role of Different Atmospheric Plasma Spray Parameters on Microstructure of Abradable AlSi-Polyester Coatings, *Solid State Phenom.*, 2017, **270**, p 224–229.
3. H.J. Xuan, N. Zhang, Y.Q. Hu, J. Shen and W.R. Hong, Evaluation of an AlSi-Polyester Abradable Seal Coating Performance Using High-Temperature and High-Velocity Abrasion Tests, *Proc. Ins. Mech. Eng. J-J Eng. Tribol.*, 2015, **230**, p 842–851.
4. S. Gao, W. Xue, D. Duan, S. Li and H. Zheng, Effect of Thermal—Physical Properties on the Abradability of Seal Coating Under High-Speed Rubbing Condition, *Wear*, 2018, **394–395**, p 20–29.
5. M.Z. Yi, B.Y. Huang and J.W. He, Erosion Wear Behaviour and Model of Abradable Seal Coating, *Wear*, 2002, **252**, p 9–15.
6. M. Öksüz and H. Yıldırım, Structure and Properties of AlSi/Polyester Coating, *J. Appl. Polym. Sci.*, 2004, **93**, p 2437–2444.
7. R. Rajendran, Gas Turbine Coatings—An Overview, *Eng. Fail. Anal.*, 2012, **26**, p 355–369.
8. Y.M. Guo, S. Zhu, Z.Y. Song, Q.G. Yu, M. Wei and J. Chen, Microstructure and Friction Behavior of AlSi/Polyester Composit-ed Coating Prepared by Subsonic Flame Spraying, *China Surf. Eng.*, 2017, **29**, p 85–90. (in Chinese)
9. T.T. Cheng, K.Y. Ding, Z.H. Ji and Z.P. Wang, Effect of Thermal Aging on Sand Erosion Resistance of AlSi Polyphony Ester Coating, *T. Mater. Heat Treat.*, 2017, **38**, p 148–154. (in Chinese)
10. Y. Duramou, R. Bolot, J.L. Seichepine, Y. Danlos, P. Bertrand, G. Montavon and S. Selezneff, Relationships between Microstructural and Mechanical Properties of Plasma Sprayed AlSi-Polyester Composite Coatings: Application to Abradable Materials, *Key Eng. Mater.*, 2014, **606**, p 155–158.
11. J.J. Tang, K. Liu, Q.Z. Yang, Y.H. Wang, P. Zhang, Y. Wang, L. Zhao, Q.Q. Fu, Z.H. Han and Y. Bai, The Influence of Size and Distribution of Graphite on the Friction and Wear Behavior of Ni-Graphite Coatings, *Surf. Coat. Technol.*, 2014, **252**, p 48–55.
12. C.H. Ding, C.H. Liu, Z.M. Yang, Y.P. Wang, Z.B. Sun and L. Yu, Effect of Size Refinement and Distribution of Lubricants on Friction Coefficient of High Temperature Self-Lubricating Composites, *Compos. Sci. Technol.*, 2010, **70**, p 1000–1005.
13. M. Yi, J. He, B. Huang and H. Zhou, Friction and Wear Behaviour and Abradability of Abradable Seal Coating, *Wear*, 1999, **231**, p 47–53.
14. Y. Bai, L. Zhao, K. Liu, J.J. Tang and Z.H. Han, Fine-Lamellar Structured Thermal Barrier Coatings Fabricated by High Efficiency Supersonic Atmospheric Plasma Spraying, *Vacuum*, 2014, **99**, p 119–123.
15. Y. Bai, Z.H. Han, H.Q. Li, C. Xu, Y.L. Xu, C.H. Ding and J.F. Yang, Structure—Property Differences Between Supersonic and Conventional Atmospheric Plasma Sprayed Zirconia Thermal Barrier Coatings, *Surf. Coat. Technol.*, 2011, **205**, p 3833–3839.
16. C. Cui, A. Schulz, K. Schimanski and H.W. Zoch, Spray Forming of Hypereutectic Al-Si Alloys, *J. Mater. Process. Technol.*, 2009, **209**, p 5220–5228.
17. X.W. Zhu, R.C. Wang, C.Q. Peng and J. Peng, Microstructure and Thermal Expansion Behavior of Hypereutectic Al-Si Alloy, *J. Cent. South Univ.*, 2016, **47**, p 1500–1505.

Publisher's Note Springer Nature remains neutral with regard to jurisdictional claims in published maps and institutional affiliations.